20

Aberrations in Confocal and Multi-Photon Fluorescence Microscopy Induced by Refractive Index Mismatch

Alexander Egner and Stefan W. Hell

INTRODUCTION

Modern optical microscopes are so good that many scientists forget that these instruments only provide their optimal performance if they are used under certain operating conditions. Typical users may be unaware of the very existence of such limitations either because they may unwittingly work within the limits or because they fail to recognize their effects. It is probably also correct to assume that the manufacturer does not intend to discourage purchase by emphasizing the pitfalls that unavoidably arise from the physics of imaging. However, advanced microscopists tend to use their instruments at the limits of their performance. They wish to use lasers from the ultraviolet (UV) to the infrared (IR), special emission lines from very large arc-lamps, charge-coupled device (CCD) cameras with a dynamic range of up to 16 bits, photon-counting avalanche photodiodes with unmatched sensitivity, and several fast photomultiplier tubes. They want to observe two or more dyes simultaneously. They expect the stage to remain in a stable position for several hours, possibly while going through heating and cooling cycles, and sometimes they want to record low-level fluorescence emissions from rather thick specimens mounted in an aqueous medium with high numerical aperture (NA) oil-immersion lenses. Is this possible? Can one expect an off-the-shelf product to perform well under all these circumstances? The answer is: Within certain limits, yes, you can. The issue is to specify and recognize these limits.

This chapter describes the problems that occur when observing specimens that are mounted in a medium whose refractive index is different from that of the immersion liquid. Classic examples are live cells kept in a physiological buffer solution or even fixed cells kept in a glycerol-based mountant that are imaged by an oil-immersion lens of large numerical aperture. This chapter first outlines the physics of the situation, both for confocal and multi-photon microscopy, then presents the results of a theoretical investigation, compares them with a series of experiments, and finally draws conclusions that are particularly relevant to the quantitative observation of (living) biological specimens.

THE SITUATION

Figure 20.1 describes a common situation encountered in microscopy. The sample is mounted between a coverslip and a glass slide, which in fact can be another coverslip, and is immersed in a special mounting medium, such as an aqueous buffer or a more viscous solution based on glycerol. Coverslip glass has a refractive index (RI) $n = 1.518$. The immersion oil between the coverslip and the objective lens is assumed to have the same n. The n of the mounting medium around the sample will usually be different from that of the glass and of the immersion oil. Water has an index of $n = 1.33$ and glycerol has $n = 1.47$. The sample itself will have an n that is not much different from that of the mounting medium and slightly higher than that of water (see Chapter 18, *this volume*, for the RIs of common mounting media).

A light ray emerging from an oil-immersion objective lens that is coupled to the coverslip with the appropriate oil will not be refracted until it passes the interface from the coverslip into the mounting medium. The light ray is usually only slightly affected by the sample itself and is assumed to carry on straight towards the focal region once it has passed the interface between the mounting medium and the coverslip. The discussion can therefore be restricted to the effects caused by the change in n at the glass–medium boundary and to the distance from this interface to the focus point somewhere inside the sample. What effects can be expected?

- A light ray is refracted at the glass–medium interface. The angle of the ray is changed; therefore, the different rays focus at different positions along the z-axis than they would in a perfectly matched optical system. In microscopy, n_1 is usually larger than n_2, and the focus is, therefore, closer to the coverslip than under ideal conditions. The position of an object will then appear to be further away from the coverslip. If n_1 were smaller than n_2, the focus would be further from the coverslip than it should be and the object would then appear to be closer to the coverslip.
- Whenever light is refracted, some light is also reflected (Born and Wolf, 2002). As refraction occurs only when the angle of incidence is lower than the angle of total internal reflection, the NA of the immersion system is effectively reduced.
- Perfect imaging is only possible if the wavefront remains spherical. Any deviation from sphericity results in a larger spread of the focus and hence in a reduction in both spatial resolution and peak intensity.
- This spreading of the focus means that the image of the focal spot focused back towards the confocal pinhole is also spread. This second defocus effect means that less light penetrates the pinhole, and the observed intensity decreases still more.

THEORY

The calculations are performed in a vectorial theory following Hell and colleagues (1992). The sample object is a layer of fluorophore immersed in the mounting medium. The immersion oil and the

Alexander Egner and Stefan W. Hell • Department of NanoBiophotonics; Max Planck-Institute for Biophysical Chemistry, Am Fassberg 11; D-37077 Goettingen, Germany

 Handbook of Biological Confocal Microscopy, Third Edition, edited by James B. Pawley, Springer Science+Business Media, LLC, New York, 2006.

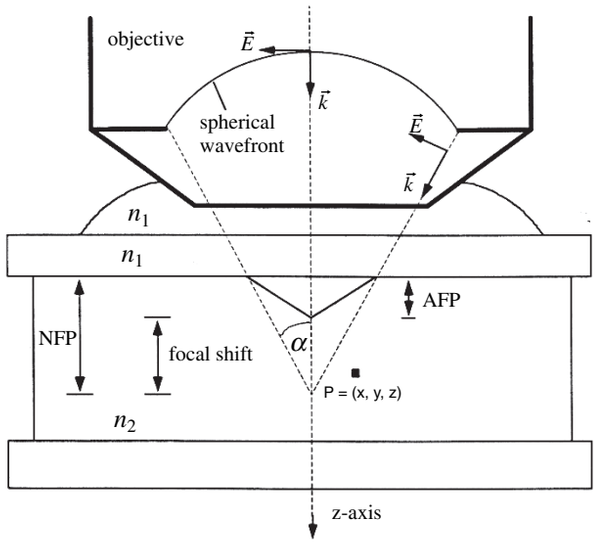

FIGURE 20.1. Terminology used for the calculation of point spread functions in optically mismatched systems. A spherical wavefront emerges from the objective lens. The wavefront is described by its electric field strength $\vec{E}$ and its direction $\vec{k}$, while the objective lens is described by its focal length and its numerical aperture (NA) = n_1 sin(α). The sample consists of two coverslips, each with a refractive index of n_1 and the mounting medium with a homogeneous refractive index of n_2. The immersion medium between the upper coverslip and the objective lens has the same n as the coverslip. In a perfectly matched system, n_1 is equal to n_2 and the geometrical focus is a distance NFP (nominal focal position) away from the glass/mounting medium interface. In a mismatched system, n_1 is not equal to n_2. The focus suffers from a focal shift and is found at AFP (actual focal position). The theory describes the calculation of the electric field strength $\vec{E}$ in a point $P(x,y,z)$ close to both AFP and NFP.

coverslip have $n = n_1$ and the mounting medium $n = n_2$. Focusing into the sample is achieved by mechanically varying the distance between the objective lens and the bottom of the coverslip. The distance between this surface and the geometrical focus in a perfectly matched system is referred to as the nominal focal position (NFP).[1] The difference between the NFP and the actual focal position (AFP) is referred to as the focal shift in the optically mismatched system. We wish to calculate the AFP and the intensity at a point $P(x,y,z)$ in the vicinity of the AFP. The optical system is described by the wavelength of the incident light ray (λ), the NA of the objective lens, and the diameter of the aperture in the lens. In a modern optically perfectly matched microscope, the so-called infinity-corrected lens is assumed to accept a perfectly planar incoming-wavefront and produce a perfectly spherical outgoing wavefront that produces an aberration free point spread function (PSF) at the focal point. We note that our considerations apply to any point within the field of view specified for the lens.

In a confocal microscope, a point source is used to define the extent and the position of illumination, whereas a point detector discriminates against any light emitted outside a certain region. In physical terms, the effective PSF (Hell *et al.*, 1992) of the confocal fluorescence microscope is given by the product of the illumination intensity and detection PSF:

$$h_{cf} = \left|\vec{h}_{ill}\right|^2 \times \left|\vec{h}_{\mathrm{det}}\right|^2 \approx \left|\vec{h}_{ill}\right|^4 \qquad \textbf{(1)}$$

where $\vec{h}_{ill}$ denotes the amplitude of the illumination light in the focal region and $\vec{h}_{\mathrm{det}}$ is the amplitude distribution for the detection, which is similar to $\vec{h}_{ill}$, but is calculated for the wavelength of fluorescence emission. So, while $\vec{h}_{ill}$ is proportional to the light field used for illumination, and $|\vec{h}_{ill}|^2$ to its intensity, the effective confocal PSF h_{cf} is proportional to the probability that a given focal coordinate contributes to the signal at the confocal detector. If the excitation and emission wavelengths are rather similar, it follows that $|\vec{h}_{ill}|^2 \approx |\vec{h}_{\mathrm{det}}|^2$. In this case, h_{cf} is proportional to the fourth power of the illumination amplitude and hence to the square of the illumination intensity (Wilson and Sheppard, 1984), as indicated on the right-hand side of Eq. 1. This quasi-quadratic signal dependence of the recorded intensity on the illumination intensity causes a drop of the detected fluorescence from points away from the geometrical focus and is the actual physical reason why a confocal setup defines a confined recording volume in three-dimensional (3D) space.

The z-response $I(z)$ to infinitely thin fluorescent planes and the response $I_{\mathrm{edge}}(z)$ to half-volumes in the z-direction are of practical importance as well because they quantify the ability of a microscope to distinguish planes that are stacked in the z-direction:

$$I(z) = \int_{-\infty}^{\infty}\int_{-\infty}^{\infty} h_{cf}(\vec{r})dx\,dy \text{ and } I_{edge}(z) = \int_{-\infty}^{z} I(z')dz' \qquad \textbf{(2)}$$

A volume confinement can also be achieved by multi-photon excitation of the fluorophores (Denk *et al.*, 1990; Sheppard and Gu, 1992a, 1992b) (Chapters 28 and 37, *this volume*). The probability of two photons being simultaneously absorbed by the same molecule is proportional to the square of the local intensity (Kaiser and Garret, 1961). Therefore, the effective PSF of a microscope based on two-photon absorption is described by the square of the illumination PSF, that is, the fourth power of the field amplitude for illumination:

$$h_{2h\nu} = \left|\vec{h}_{ill}\right|^4 \qquad \textbf{(3)}$$

The similarity to Eq. 1 indicates that the illumination process defines a volume in a manner similar to the combined illumination and detection processes in a confocal single-photon excitation fluorescence microscope (Hell and Stelzer, 1992; Sheppard and Gu, 1992b; Stelzer *et al.*, 1994). This means that all the problems discussed for single-photon confocal microscopy are also encountered in two-photon fluorescence microscopes. The only real difference is that the latter requires wavelength doubling. Additional confocalization of the system means that the effective PSF is given by $h_{cf\,2h\nu} = |\vec{h}_{ill}|^4 \times |\vec{h}_{\mathrm{det}}|^2$ and for an n-photon confocalized system we obviously have

$$h_{cf\,2h\nu} = \left|\vec{h}_{ill}\right|^{2n} \times \left|\vec{h}_{\mathrm{det}}\right|^2. \qquad \textbf{(4)}$$

In an aberration-free system, the calculation of the fields $\vec{h}_{ill}$ and $\vec{h}_{\mathrm{det}}$ is rather straightforward because these functions solely depend on the wavelength and the NA. By contrast, when focusing through RI interfaces, the evaluation of $\vec{h}_{ill}$ and $\vec{h}_{\mathrm{det}}$ is complicated by the fact that, loosely speaking, it has to be calculated once for medium n_1 and then for medium n_2 (Hell *et al.*, 1993). The latter publication treated the problem with specific regard to confocal microscopy and quantitatively predicted all the effects

[1] It should be noticed that the NFP is the actual distance of a feature in the object from the surface of the coverslip.

encountered with refractive index mismatched samples. Therefore, in this chapter we will follow the argument presented in that publication. In the meantime, significant advancements in the formulation of this theory have been made. These are considered later in this chapter (Török *et al.*, 1995; Egner and Hell, 1999).

Starting from simple terms, the calculation basically requires the solution of a variational problem in optics, that is, the application of Fermat's principle from a point of the converging spherical wavefront to the point of the focal region in question [Fig. 20.2(A)]. According to the Huygens–Fresnel construction, each point on the spherical wavefront is a source of secondary spherical wavelets (Hopkins, 1943; Li and Wolf, 1981). In a matched medium, we have

$$\vec{h}(\vec{r}) = c\int_F\int \vec{A}(F)\frac{1}{s}K(\chi)\exp(iks)dF \tag{5}$$

where $\vec{A}(F)$ denotes the wavefront amplitude over the surface F of the spherical wavefront and dF is the surface element (see Fig. 20.2); s is the distance between the origin of the wavelet q and the point P, and χ is the angle of inclination between the normal at q and the direction from q to P.

$$K(\chi) = -\frac{1}{2\lambda}(1+\cos(\chi)) \tag{6}$$

In an aplanatic objective lens, the wavefront $\vec{A}(F)$ is given for in the x-direction polarized light of Amplitude A_i by Richards and Wolf (1959):

$$\vec{A}(F) = A_i\sqrt{\cos(\theta)}\begin{pmatrix}\cos(\theta)+(1-\cos(\theta))\sin^2(\varphi)\\(1-\cos(\theta))\cos(\varphi)\sin(\varphi)\\\sin(\theta)\sin(\varphi)\end{pmatrix} \tag{7}$$

For the numerical calculation of $\vec{h}(\vec{r})$, the term $K(\chi)$ can be neglected because it varies by only a small amount. Because the calculation is restricted to the volume close to the geometrical focus, $1/s$ remains a constant and can therefore also be neglected. The function $\vec{h}(\vec{r})$ can be simplified to

$$\vec{h}(\vec{r}) = c\int_0^a\int_0^{2\pi}\sqrt{\cos(\theta)}\begin{pmatrix}\cos(\theta)+(1-\cos(\theta))\sin^2(\varphi)\\(1-\cos(\theta))\cos(\varphi)\sin(\varphi)\\\sin(\theta)\sin(\varphi)\end{pmatrix}\exp(iks)\sin(\theta)d\varphi\, d\theta \tag{8}$$

The final problem is the determination of s, which, as is pointed out above, is a variational problem and a careful analysis of the light transition at the interface between n_1 and n_2, to which one solution has been provided (Hell *et al.*, 1993).

If the NFP is small compared to the focal length of the objective lens, an assumption which is well met in confocal microscopy, the variational problem can be solved analytically for the region near the NFP (Egner and Hell, 1999). Török and colleagues derived an identical solution (Török *et al.*, 1995) using a plane wave expansion of the light field, that is, the Debye approximation instead of the Huygens–Fresnel construction. In both cases the solution for $\vec{h}(\vec{r})$ is given by:

$$\vec{h}(\vec{r}) = c\begin{pmatrix}i(I_0(\vec{r})+I_2(\vec{r})\cos(2\varphi))\\I_2(\vec{r})\sin(2\varphi)\\i\,2I_1(\vec{r})\cos(\varphi)\end{pmatrix} \tag{9}$$

Where the diffraction integrals I_n are defined by:

$$\begin{aligned}
I_0 &:= \int_0^a \sqrt{\cos(\theta_1)}\sin(\theta_1)\left(\tau_s+\tau_p\cos(\theta_2)\right)J_0\left(kn_1\sqrt{x^2+y^2}\sin(\theta_1)\right)\\
&\quad \exp(ik(\Phi(NFP)+n_2z\cos(\theta_2)))d\theta_1\\
I_1 &:= \int_0^a \sqrt{\cos(\theta_1)}\sin(\theta_1)\left(\tau_p\sin(\theta_2)\right)J_1\left(kn_1\sqrt{x^2+y^2}\sin(\theta_1)\right)\\
&\quad \exp(ik(\Phi(NFP)+n_2z\cos(\theta_2)))d\theta_1\\
I_2 &:= \int_0^a \sqrt{\cos(\theta_1)}\sin(\theta_1)\left(\tau_s-\tau_p\cos(\theta_2)\right)J_2\left(kn_1\sqrt{x^2+y^2}\sin(\theta_1)\right)\\
&\quad \exp(ik(\Phi(NFP)+n_2z\cos(\theta_2)))d\theta_1
\end{aligned} \tag{10}$$

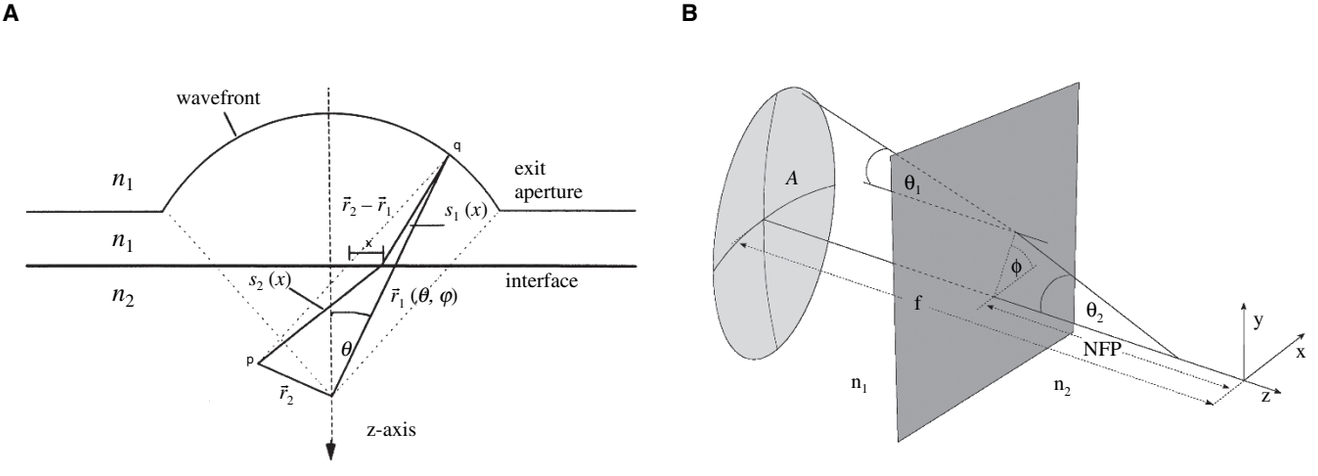

FIGURE 20.2. (A) The variational approach to the calculation of the electric field strength $\vec{E}$ at a point $P(x,y,z)$ close to both the AFP and the NFP. The geometry is basically the same as described in Figure 20.1. The problem is to minimize the distance $s_1(x) + s_2(x)$. It can be shown that this sum depends on the angle and on the origin of the beam in the primary spherical wavefront. The calculation, therefore, has to search for those beams that contribute to the field at position P according to Fermat's principle. For each point P(x,y,z) in the object, the contribution is found by integrating the complex electric field across the whole exit aperture. This makes the calculations somewhat tedious. (B) If the NFP is small compared to the focal length of the objective lens, which is always the case in microscopy, the calculation becomes much easier as only the transmission and refraction for a beam incident upon the boundary with an angle θ_1 has to be known.

J_n are Bessel functions of the first kind and nth order and $\tau_{p,s}$ are Fresnel transmission coefficients for s- and p-polarized light (Born and Wolf, 2002). The aberration function

$$\Phi(NFP) = -NFP(n_1 \cos(\theta_1) - n_2 \cos(\theta_2)) \quad \textbf{(11)}$$

depends on the nominal focusing position, the azimuth angle θ and therefore on the aperture angle α and the difference of the refractive indices n_1 and n_2. The differences between the calculations of the illumination and the detection PSFs are the wavelength and the term $\sqrt{\cos(\theta)}$ which is omitted.

RESULTS OF THEORETICAL CALCULATIONS

The theory described above does not result in an analytical description of the PSF. The PSFs have to be calculated numerically as a function of the NA, excitation and emission wavelengths, NFP, n_1, and n_2. In order to illustrate how focusing into a mismatched medium affects the PSF, Figure 20.3 shows xz-images of calculated PSFs (logarithmic scale) and the corresponding experimental through-focus series (linear scale) for focusing with a water-immersion lens either 10 µm deep into water [Fig. 20.3(A,B)] or into immersion oil [Fig. 20.3(C,D)]. In the mismatched case, the main maximum is shifted, becomes relatively broader, and drops in peak intensity (Fig. 20.4). In addition, the PSF loses its axial symmetry with respect to the main maximum whereby focusing above the AFP leads to a different image from focusing below the AFP [Fig. 20.3(D)], an effect that is not present in the matched case [Fig. 20.3(B)].

The results of several calculations are summarized in Figures 20.4, 20.6, 20.7, 20.8, 20.9, and 20.10 and in Tables 20.1 and 20.2 for water and for glycerol mounting media. Figure 20.4 shows the integrated intensity for various NFPs using water as the mounting medium. The first image indicates the ideal situation encountered with a fluorophore mounted in immersion oil. The following images show again that the integrated intensity is smeared along the optical axis, and an additional peak appears below the main maximum. The main maximum itself is shifted, drops in peak intensity, and becomes relatively broader. These values can be evaluated to obtain the focal shift [(NFP) – (AFP)], the drop in peak intensity, and the full-width half-maximum (FWHM) of the main peak. While, because of its convoluted shape (Fig. 20.5), it is difficult to specify a simple metric that quantifies the sharpness of a spherically aberrated focal spot, the FWHM of the main peak is relatively simple to measure and hence has become the most common measure of the xy or axial resolution.

Calculations for some numbers encountered in real situations have been combined with the experimental results in Figures 20.6, 20.7, and 20.8. Figure 20.9 shows the focal shift of the excitation PSF of a 0.6 oil-immersion objective lens directly as a function of NFP for various refractive indices. Figure 20.10 also plots the focal shift but for an NA 1.4 oil-immersion objective lens. The AFP is regarded as the position of the global maximum of the PSF along the optical axis rather than the center of gravity or some other measure of this complex shape.

An important result of these calculations is that the effects of spherical aberration increase rapidly with $(n_1 - n_2)$, NA, and distance of the object from the coverslip (NFP). As long as the

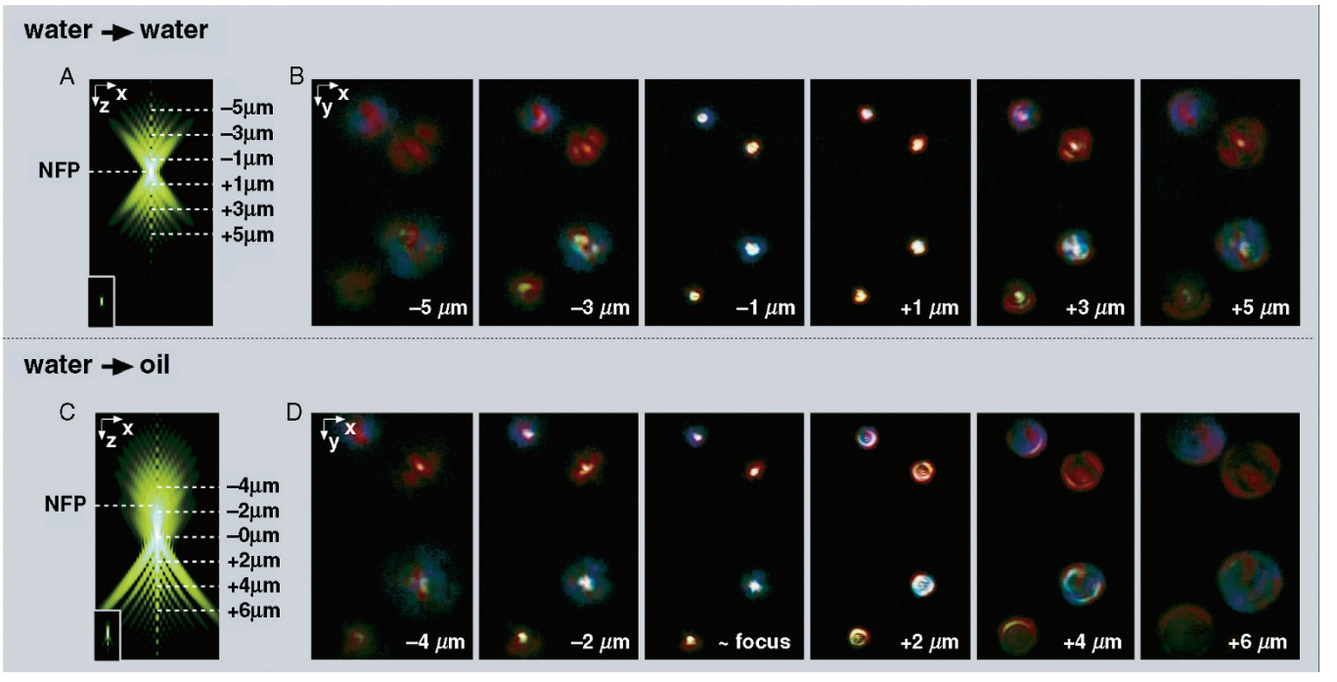

FIGURE 20.3. Influence of a mismatched medium on the PSF. (A) and (C) show xz-images of calculated PSFs in logarithmic scale for focusing with a water-immersion lens (n = 1.334) 10 µm deep into water and immersion oil (n = 1.518), respectively. The inlets in the lower left corners show the central part of the PSFs in linear scale. (B) and (D) show corresponding experimental through-focus series in a linear scale. These series represent exactly what one would see when focusing through a point-like object. Focusing into a mismatched medium causes a shift and a broadening of the main maximum. The aberrated PSF can be clearly identified in the through-focus series as focusing above the AFP leads to a different image from focusing below the AFP. The image series was made of a mirror specimen by J. Pawley using a Zeiss Axioskpp 50, with a 40×/NA1.2 C-Apo objective, and recorded with a Sony TRV-900 camcorder using the zoom lens to provide the high magnification.

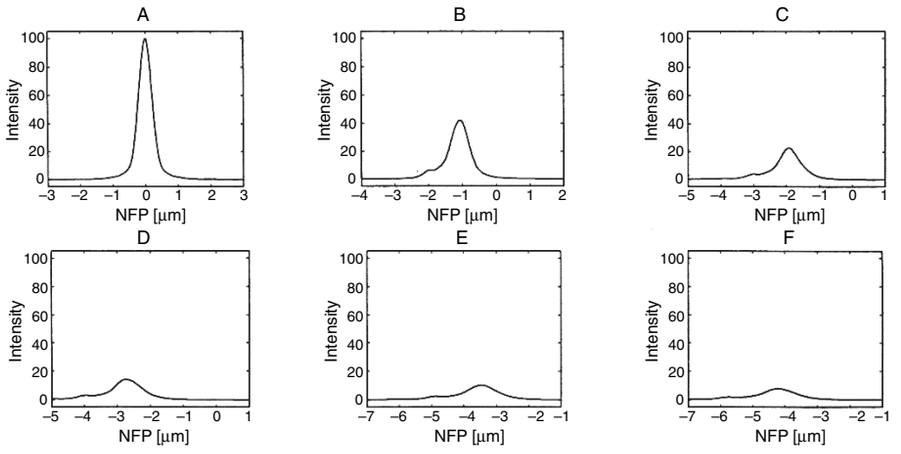

FIGURE 20.4. Integrated z-responses for various penetration depths (NFP) in water for an NA = 1.3 oil-immersion objective lens. The excitation and emission wavelengths were 514 nm and 590 nm, respectively. (A) Ideal situation in oil, penetration depths of (B) 5 μm, (C) 10 μm, (D) 15 μm, (E) 20 μm, and (F) 25 μm. All curves are normalized to the ideal situation encountered with immersion oil as the mounting medium. The point spread function is obviously not confined to the minimal volume but instead continues to spread the larger NFP becomes. This causes a decrease of the maximal intensity, an increase of the full-width half-maximum, and a focal shift. The intensity is distributed among several axial peaks of which at least two are clearly visible. Please note that the NFP axis has been offset.

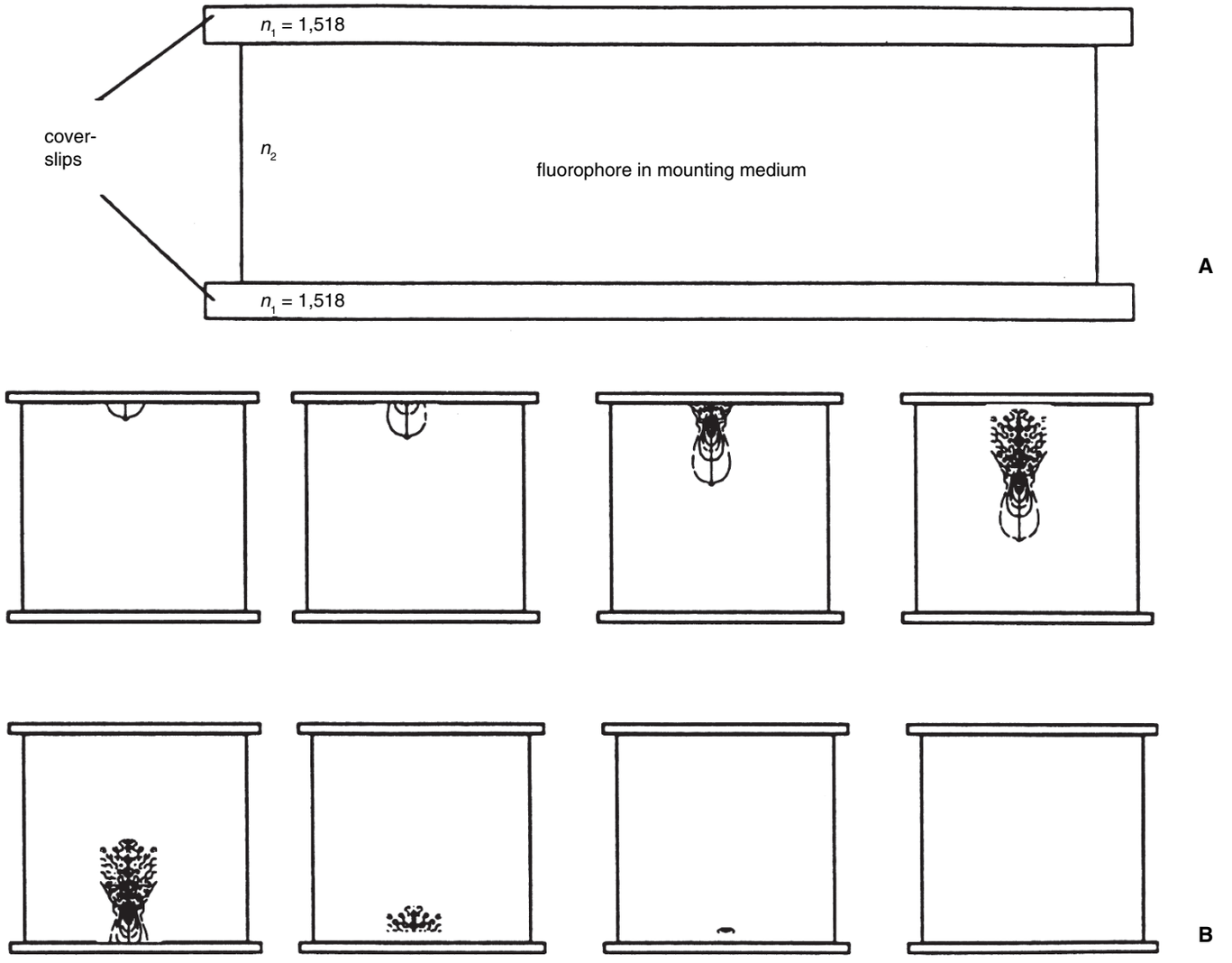

FIGURE 20.5. Sample used for measuring the edge response in a confocal laser-scanning microscope. (A) The sample consists of two coverslips or a coverslip and a glass slide with a fluorophore dissolved in the mounting medium (water, glycerol, immersion oil) in between. The sample thickness (upper/lower interface distance) is at most 100 μm. In this sample, the concentration of the fluorophore is zero inside the glass and abruptly reaches a high concentration when moving the probe along the optical axis. (B) During the experiment, the point spread function penetrates the mounting medium through a coverslip. The measured fluorescence intensity signal depends on the penetration depth. The fluorescence emission is maximal when the point spread function is completely inside the sample. Because the point spread function has a finite size, it has a response curve with a finite steepness. The slopes close to the interfaces can, therefore, be used to determine the extent of the point spread function along the optical axis, and this is the axial resolution of the instrument.

TABLE 20.1. Result of Calculations for Glycerol[a,b]

NFP (μm)	Focal Shift (μm)	Normalized Intensity	Axial Edge FWHM (μm)	Axial PSF FWHM (μm)	Lateral PSF FWHM (μm)
0	0	100	0.53	0.47	0.16
5	–0.28	95	0.53	0.47	0.16
10	–0.55	91	0.53	0.47	0.16
15	–0.83	78	0.555	0.47	0.16
20	–1.10	62	0.65	0.50	0.18
25	–1.33	50	0.81	0.57	0.18
30	–1.54	40	0.97	0.77	0.20
50	–2.30	31	1.00	0.72	0.20

[a] For various nominal focal positions (NFP), the focal shift, the normalized intensity, the axial edge response, the axial width of the PSF, and the lateral width of the PSF have been calculated for an NA = 1.3 oil-immersion objective lens and excitation and emission wavelengths of 514 nm and 590 nm, respectively.
[b] The values for an NFP = 0 are the ideal values if immersion oil is used as the mounting medium.

TABLE 20.2. Result of Calculations for Water[a]

NFP (μm)	Focal Shift (μm)	Normalized Intensity	Axial Edge FWHM (μm)	Axial PSF FWHM (μm)	Lateral PSF FWHM (μm)
0	0	100	0.53	0.47	0.16
5	–1.0	60	0.68	0.58	0.20
10	–1.83	39	0.90	0.70	0.20
15	–2.57	28.50	1.08	0.88	0.23
20	–3.30	23	1.22	0.93	0.24
25	–4.02	19	1.37	1.00	0.24
30	–4.72	16.60	1.45	1.11	0.24
50	–7.57	11	1.79	1.37	0.24

[a] For various nominal focal positions (NFP), the focal shift, normalized intensity, axial edge response, axial width of the PSF, and lateral width of the PSF have been calculated for an NA = 1.3 oil-immersion objective lens and excitation and emission wavelengths of 514 nm and 590 nm, respectively. The values for an NFP = 0 are the ideal values if immersion oil is used as the mounting medium.

spherical aberrations are below a certain threshold, the focal shift depends linearly on the NFP which can be used to correct the apparent thickness of a sample. If the spherical aberrations exceed the threshold, the relation between the NFP and the focal shift becomes nonlinear which leads to image distortions along the *z*-axis and a rapid drop in intensity as the excitation and emission PSF will be substantially displaced. This effect is most prominent with high NAs and very low for oil-immersion lenses having an NA of <0.85.

EXPERIMENTS

To verify these calculations, Rhodamine 6G was dissolved in water, glycerol, and immersion oil to form ~10^{-5} *M* solutions. The solutions were mounted between a glass slide and a coverslip using droplets of dried nail polish as spacers. The samples were placed either onto a home-built confocal microscope (Stelzer *et al.*, 1991) [Figs. 20.6, 20.7(A), 20.8] or a commercial confocal microscope (TCS SP2, Leica Microsystems Heidelberg, Mannheim, Germany) (Martini *et al.*, 2002) [Fig. 20.7(B)]. The dye was excited at a wavelength of 488 nm and observed either above 530 nm [Figs. 20.6, 20.7(A), 20.8] or between 495 nm and 530 nm [Fig. 20.7(B)]. For the data presented in the Figures 20.6, 20.7(A) and 20.8, a Zeiss Apochromat 100× oil objective with an adjustable aperture (NA 0.8–1.4) was used, whereas the data of Figure 20.7(B) was recorded with a 100× adjustable aperture Leica oil-immersion lens (HCX PL APO 1.4–0.7) and a 100×, 1.35 NA Leica glycerol-immersion lens (HCX PL APO, GLYC CORR). The instruments were used to record *xz*-images, that is, images in a plane parallel to the optical axis (Fig. 20.5). These images started with the focus in the coverslip and ended with the focus in the glass slide. The

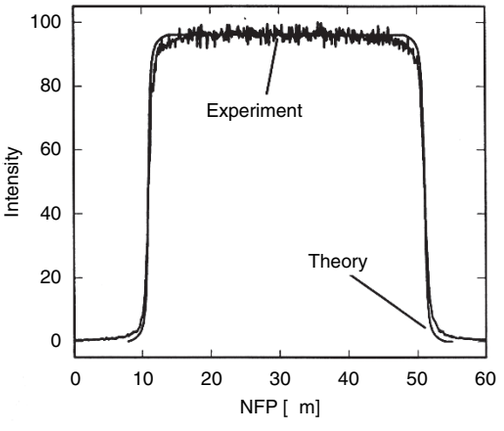

FIGURE 20.6. The experimental and the theoretical edge-response curves for immersion oil. The theoretical curve was fitted to the experimental data set to comply with the apparent sample thickness and the maximum intensity in the sample. The theoretical calculations assume a perfect match of the refractive indices of the immersion oil, the glass, and the mounting medium. As shown, this condition is almost, but not perfectly, fulfilled under real conditions. The theory predicts a slightly steeper slope.

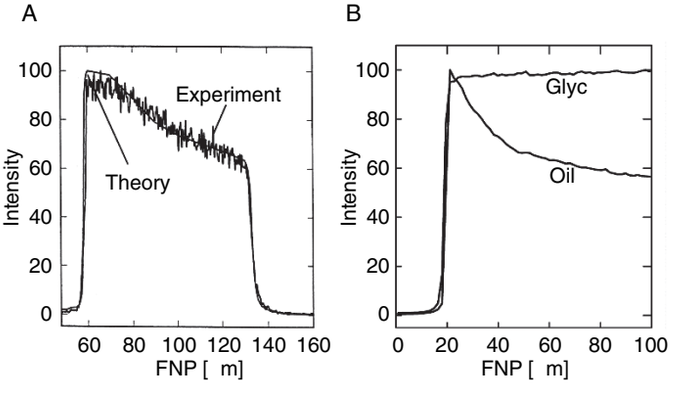

FIGURE 20.7. The experimental and the theoretical edge-response curves for glycerol. Focusing with an oil-immersion lens into glycerol leads to a significant drop in image brightness (A). The theoretical curve was fitted to the experimental data set to comply with the apparent sample thickness and the maximum intensity in the sample. The intensity decrease is perfectly reproduced. (B) By using a glycerol-immersion lens the drop in image brightness can be prevented.

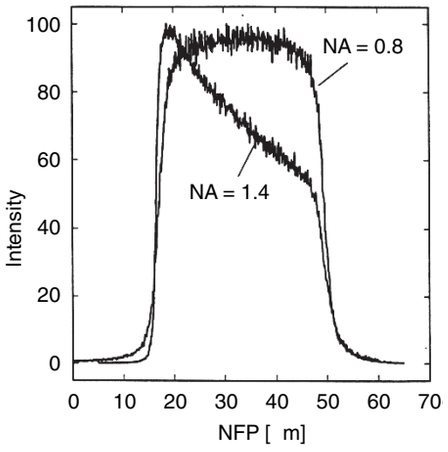

FIGURE 20.8. Two edge-response curves in a water sample. The graph shows the intensities as a function of NFP for NA 1.4 and 0.8. Both curves were recorded with the same sample in the same position. This is possible because the objective lens (Zeiss Plan-Apochromat 100×, NA 1.4) has an adjustable NA. The figure demonstrates that the loss in resolution and the loss in intensity are due to the effects of high NA and not to quenching or bleaching.

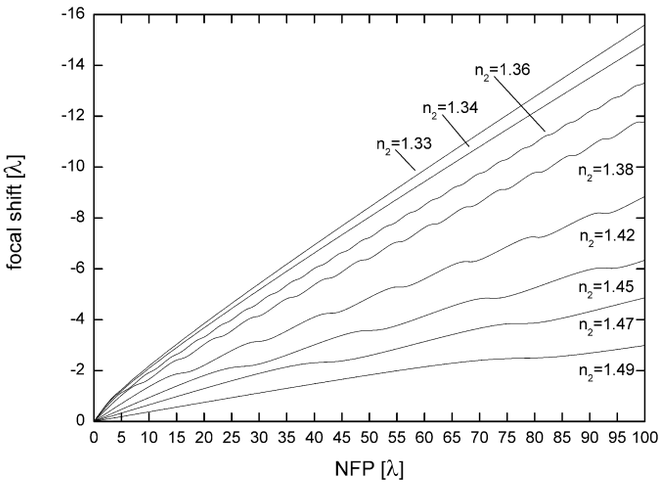

FIGURE 20.10. Dependence of the focal shift for an NA = 1.4 oil-immersion objective lens on the nominal focal position for various refractive indices between 1.33 and 1.49. For such a high NA objective lens, the variation is only linear up to a certain maximum NFP, which strongly depends on the difference in the refractive index and the aperture angle. After that, the focal shift starts to show some kind of oscillation. In the linear regime the curves can be used to correct the apparent thickness of a sample in a mounting medium with a known refractive index by multiplying it by an appropriate factor.

64 central columns were then averaged to generate the edge-response curves (see Eq. 6) shown in Figures 20.6 through 20.8. These graphs resemble intensity signals as a function of the NFP. Of interest is the edge steepness on both sides and the variation in peak intensity with depth. The results are summarized in Table 20.3. Because it was not possible to systematically vary the thickness of the dye layer (usually between 50 µm and 100 µm), the focal shift was not measured directly.

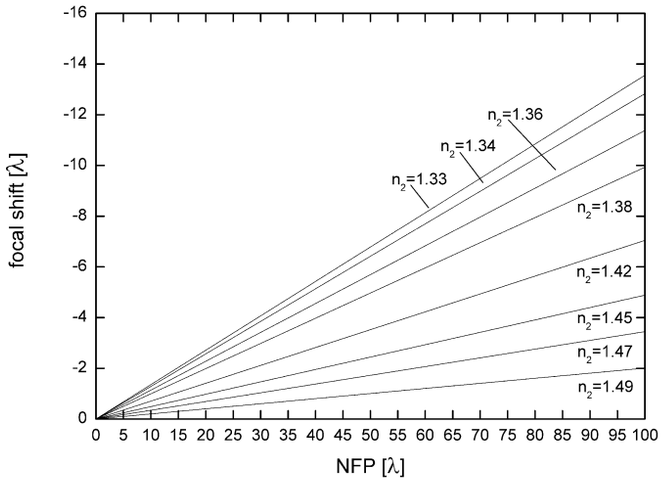

FIGURE 20.9. Dependence of the focal shift for an NA = 0.6 oil-immersion objective lens on the nominal focal position for various refractive indices between 1.33 and 1.49. For such a low NA objective lens, the variation is linear for the whole range. The curves can be used to correct the apparent thickness of a sample in a mounting medium with a known refractive index by multiplying it by an appropriate factor.

OTHER CONSIDERATIONS

Dry Objectives

The use of dry, high-NA lenses for the observation of wet specimens, or even those sealed behind glass coverslips, causes aberrations that are much worse than for any of the situations described above.

First, the difference between the refractive indices of the immersion and embedding media is larger than for any other type of objective. Therefore, focusing even a few micrometers into the sample will result in a severe drop of intensity and resolution. Of course, this can be avoided by adjusting the correction collar. Most high-NA dry objectives are equipped with such a collar but the correct adjustment only works for a single plane. Every change of the NFP will result in serious degradation of the PSF. For the same reason, dry objectives are very sensitive to the coverslip thickness.

Second, due to total internal reflection, the maximum angle transmitted as the emerging light moves from glass to air is 41° and 49° as it moves from water to air. The PSF is therefore dominated by the illumination PSF. The situation is much relaxed when using lenses having an NA of 0.6 or less because the angle inside the water layer is then 26° and relatively uncritical. On the other

TABLE 20.3. Result of the Experiments with Water and Glycerol

	Water (NA = 0.8)	Water (NA = 1.3)	Glycerol (NA = 1.3)
Upper edge (µm)	1.5	1.0	1.0
Lower edge (µm)	2.0	5.7	2.3
Ratio upper/lower	1.3	5.7	2.3

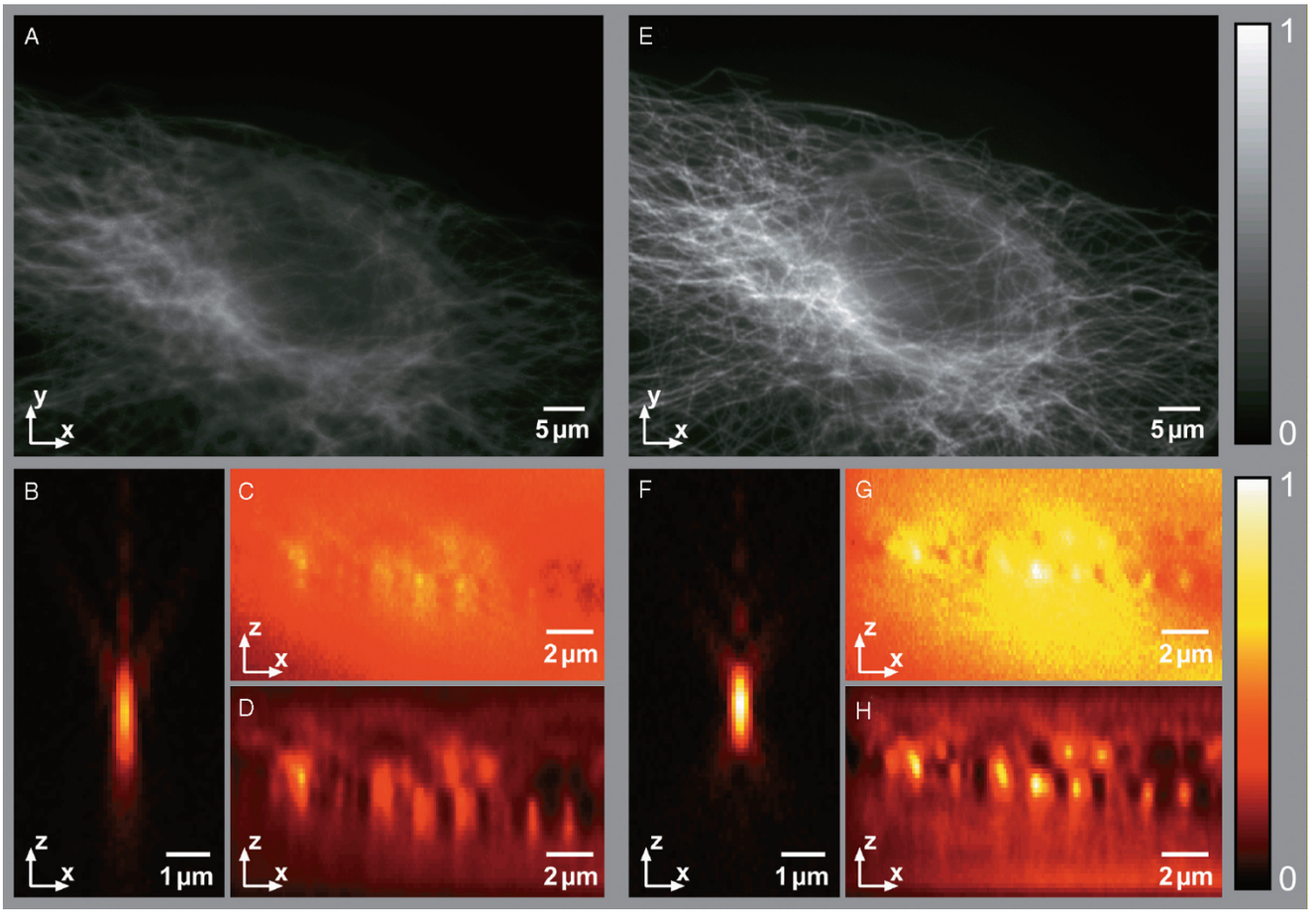

FIGURE 20.11. Optical spherical aberration correction. Images of aqueous PTK2 cells stained with Oregon green anti-tubulin and made using an NA 1.4 oil objective. Replacing microns of glass by water introduces distinct spherical aberrations [(A) *xy* image; (B) *xz* PSF; (C) raw *xz* image; (D) deconvolved *xz* image] that are not present in the corrected images [(E) *xy* image; (F) *xz* PSF; (G) raw *xz* image; (H) deconvolved *xz* image]. The loss in peak intensity and contrast is clearly visible in the images of the same *xy* plane (A,E). The *zx* images of the fluorescent microsphere show the asymmetry in the *z* direction and the loss in axial resolution (B,F). As a result, after deconvolution, tubulin fibers lying on top of each other can be clearly distinguished only in the unaberrated case.

hand, the axial resolution improvement produced by confocal microscopy under these conditions is so low that it is fair to ask if it makes sense to use such a microscope under these circumstances.

Refractive Index, Wavelength, and Temperature

The refractive index is not a constant but depends on the wavelength (a phenomenon referred to as dispersion) and on the temperature of the medium (especially with liquids). Standard immersion oil has a refractive index of 1.518 at the n_e line of the Hg spectrum (486 nm) and a temperature of 23°C, but performance away from these standard conditions may vary depending on the manufacturer of the oil. Perfect imaging is, therefore, not straightforward to achieve. Special immersion oils and gels with many different RI and varying temperature behavior are available through Cargille Laboratories (Cedar Grove, NJ).

Spherical Aberration Correction

The loss in intensity and resolution caused by RI mismatch induced spherical aberrations can highly degrade the imaging process. Therefore, it is advisable to reduce the RI mismatch as much as possible (see section Consequences). Unfortunately, this is not always possible in a specific experimental setting. For example, when using dipping water-immersion objective lenses together with a coverslip, the spherical aberrations caused by the water–glass–water transitions induce spherical aberrations that are much stronger than those shown in the preceding examples. Fortunately, it is possible to cancel out aberrations emerging at one point in the imaging process by introducing negative aberrations at another point. For example, in water-immersion objective lenses, this is done inside the lens and the spherical aberration can be adjusted using a correction collar. Of course this balancing can also be performed anywhere else in the optical path by either using a deformable mirror (Booth *et al.*, 2002), or a spatial light modulator or altering the effective tube length (Sheppard and Gu, 1992b). While the first two approaches can also correct for non-spherical aberrations, the latter can only be used for balancing spherical aberrations. Figure 20.11 shows an example for aberration correction by altering the effective tube length through a commercially available system (SAC, Intelligent Imaging Innovations Inc., Denver, CO).

Replacing micrometers of glass by water results in pronounced spherical aberration. One can recognize the severe loss in intensity and contrast in Figure 20.11(A,E), an *xy* image of tubulin in PTK2 cells stained with Oregon green. The axial resolution is also

strongly reduced [Fig. 20.11(B,F)], an effect that be compensated for by deconvolution only approximately (see Chapter 24, *this volume*). While in the aberrated case, it is difficult to distinguish individual fibers lying near each other [Fig. 20.11(C,D)], they are well separated in the aberration-free images [Fig. 20.11(G,H)].

It is important to point out that much of the charm of correcting spherical aberration by moving optical components that are not mounted in the objective lens comes from the fact that the motion of such a correcting element can now be driven by a motor.[2] As all optical devices that change the spherical correction of an optical system by tube length alteration also change its focal length, changing the correction implies creating a shift in the focal plane. However, if the motion of the corrector is driven by a computer, this same computer can also adjust the focus control in a compensatory direction to maintain the focus plane. The SAC is the first device to do this automatically. One hopes that such devices may soon be incorporated into microscope stands as a standard attachment, similar to a magnification shifter or a Bertrand lens.

CONCLUSION

The effects mentioned in this chapter are so important that most practicing microscopists will have already encountered them. The effects are mainly visible when using lenses with a high NA or, more correctly, when using lenses whose cone angle is larger than 40°. Some of the older confocal microscopes did not fill the back-focal plane completely (see Chapter 2, *this volume*) and the higher angles were basically not present, especially when using high-NA objectives of relatively low magnification (–40×), as such lenses have very large entrance pupils. Therefore, it can be assumed that these problems will become more obvious as the quality of the instruments improves and more scientists work with aqueous specimens.

Consequences

The qualitative relevance of these experiments for the observation of thick specimens mounted in an aqueous medium with a high-NA, oil-immersion objective in a confocal microscope is as follows:

- There is a serious loss of intensity when recording optical sections in focal planes away from the coverslip and this loss becomes greater as the distance from the coverslip increases.
- The PSF suffers from a serious axial smearing; consequently, the axial resolution is lower.
- The *xy*-resolution is also lower because the high-NA rays no longer reach the focal spot.
- Less fluorescence intensity is detected behind the confocal pinhole.
- The distances measured along the optical axis are smaller than the geometrical distances in the object. The benchmark to remember is that in water, the focal shift is 13λ at a penetration depth of 100λ.
- In a mismatched system, the only part of the specimen that can be observed without the severe effects described above is that immediately next to the coverslip.
- The problem is encountered in every single-photon confocal and two-photon scanning microscope.

The physical relevance of these experiments is that, in the case of a noticeably mismatched sample, a single PSF, or a single optical transfer function (OTF) is not valid throughout the sample. As the PSF or OTF can be defined only locally, a global deconvolution to remove the effect of spherical aberration using the system response is unlikely to be successful.

This chapter also shows that an aberrated PSF can be accurately calculated from an initial unaberrated PSF. The deviations follow an approximately linear relationship, and a simple linear expansion is likely to be able to describe the PSF in different locations of the object fairly well. However, this does not mean that the effect can be easily corrected. If not counteracted optically, the loss in signal level and resolution cannot be recalled.

Practical Strategies to Reduce Refractive Index Mismatch

The biologist can avoid these problems by adhering to the following guidelines:

- Always use the appropriate objective lens. High resolving objective lenses like NA 1.4 oil-immersion lenses are usually designed to be used for thin specimens mounted behind a coverslip. For other experimental settings, like imaging through the bottom of a petri dish, there are other more appropriate lenses available, particularly those that incorporate a correction collar for spherical aberration minimization. These should always be properly adjusted.
- Thick specimens should only be observed in matched systems. This means the RI of the mounting medium and the immersion medium should be identical at all wavelengths of interest. Therefore, water-immersion and glycerol-immersion lenses should be used for water- and glycerol-embedded specimens, respectively.
- Avoid situations in which the sample is thin but far away from the coverslip. This often happens when the object is either attached permanently to the glass microscope slide or when viewing cells grown on filters but separated from the protective coverslip by an unknown amount of aqueous medium.
- If you cannot match the RI of the mounting medium to that of the immersion, try to get its refractive index as similar as possible. This can be accomplished by preparing mixtures of glycerol and water or by adding large amounts of dextrose to the mounting medium. This will at least reduce the amount of spherical aberrations incident at a certain focusing depth.
- For unmatched systems, increase the size of the detection pinhole as a function of the penetration depth. This will not improve the PSF, but it will increase the detectable signal without any further losses in resolution, and at least the brightness will not decrease so much as the image series extends farther from the coverslip surface.
- If you have to image deeper into unmatched samples and no appropriate lens is available, use a lower NA immersion objective. As demonstrated in Figure 20.8, for small mismatches, the loss in intensity is much less below NA 0.85. However, the lower NA has its own disadvantages: lower light collection and lower resolution. As shown in Table 20.3, looking through

[2] Other methods proposed for the automatic correction of spherical aberrations include deformable mirrors and spatial light modulators. Like the SAC, these devices would be introduced after the objective, where their operation could be computer controlled and any adjustments could be coupled with any changes in stage position that might be required.

50 µm of aqueous specimen with an NA 1.4 oil lens decreases the axial resolution by a factor of 6 and the intensity becomes as low as 11%. If you use instead a NA 0.8 lens, the axial resolution at the surface will be $(0.8/1.4)^2 = 3$ times worse and only 36% of the fluorescence photons of the oil lens will be collected due to the smaller aperture angle. At an imaging depth of 50 µm things will have changed: The peak light intensity will drop to only about 33%, which is about the same signal as we would get with the oil lens (36% * 33% = 12%) and the resolution will be 6 / (3 * 1.3) = 1.5 times that of the oil lens. Clearly, this is an improvement, and the advantage becomes even more prominent as the sample becomes thicker. On the other hand, imaging through a 20 µm layer of water gives about the same image with either lens, and any features closer to the coverslip will be imaged better by the larger NA lens. Of course, one must keep in mind that imaging through ~10 µm of water with an oil immersion lens leads to a seriously aberrated PSF.

- Spherical aberration (and *not* absorption) is the major source of the reduction in fluorescence signal with focus depth commonly noted by most practicing confocal microscopists.
- Optimal observation of thick living specimens occurs when the sample is observed using water-immersion objectives and no coverslip. Upright microscopes are best suited for this purpose because the water is then less likely to leak into the objective. However, the absence of a coverslip may cause the specimen to move as the focus plane changes to record 3D data. Under these conditions, one may be able to use either water-immersion lenses corrected for use with a coverslip (see Chapter 7, *this volume*) or CYTOP plastic coverslips, which have $n = 1.34$, and as a result can be used with normal water-immersion lenses.
- If the experimental setting does not allow for spherical aberration minimization, think about aberration balancing inside the optical light path by introducing a spherical aberration correction device.

ACKNOWLEDGMENTS

This chapter is in part based on Chapter 20 of the previous edition. We acknowledge earlier suggestions and contributions by Gernot Reiner and Ernst Stelzer. We thank Julia König and Nicole Zobiack from Intelligent Imaging Innovations for granting us access to the spherical aberration corrector, Scientific Volume Imaging for providing us with their Huygens deconvolution software, Andreas Schönle for providing us with his image acquisition and analysis software Imspector, Jaydev Jethwa for carefully proofreading the manuscript, and all the members of the Department of NanoBiophotonics and James Pawley for valuable discussions.

REFERENCES

Booth, M.J., Neil, M.A.A., Juskaitis, R., and Wilson, T., 2002, Adaptive aberration correction in a confocal microscope, *Proc. Natl. Acad. Sci. USA* 99:5788–5792.

Born, M., and Wolf, E., 2002, *Principles of Optics*, Cambridge University Press, Cambridge, New York.

Denk, W., Strickler, J.H., and Webb, W.W., 1990, Two-photon laser scanning fluorescence microscopy, *Science* 248:73–76.

Egner, A., and Hell, S.W., 1999, Equivalence of the Huygens-Fresnel and Debye approach for the calculation of high aperture point-spread-functions in the presence of refractive index mismatch, *J. Microsc*. 193:244–249.

Hell, S.W., and Stelzer, E.H.K., 1992, Fundamental improvement of resolution with a 4Pi-confocal fluorescence microscope using two-photon excitation, *Opt. Commun*. 93:277–282.

Hell, S.W., Lehtonen, E., and Stelzer, E.H.K., 1992, Confocal fluorescence microscopy: Wave optics considerations and applications to cell biology, In: *Visualization in Biomedical Microscopies: 3-D Imaging and Computer Applications* (A. Kriete, ed.), VCH, Weinheim, Germany, pp. 145–160.

Hell, S.W., Reiner, G., Cremer, C., and Stelzer, E.H.K., 1993, Aberrations in confocal fluorescence microscopy induced by mismatches in refractive index, *J. Microsc*. 169:391–405.

Hopkins, H.H., 1943, The Airy disc formula for systems of high relative aperture, *Proc. Phys. Soc*. 55:116.

Kaiser, W., and Garret, C.B., 1961, Two-photon excitation in CaF2:Eu2+, *Phys. Rev. Lett*. 7:229–231.

Li, Y.W., and Wolf, E., 1981, Focal shifts in diffracted converging spherical waves, *Opt. Commun*. 39:221–215.

Martini, N., Bewersdorf, J., and Hell, S.W., 2002, A new high-aperture glycerol immersion objective lens and its application to 3D-fluorescence microscopy, *J. Microsc*. 206:146–151.

Richards, B., and Wolf, E., 1959, Electromagnetic diffraction in optical systems II. Structure of the image field in an aplanatic system, *Proc. R. Soc. Lond. A* 253:358–379.

Sheppard, C.J.R., and Gu, M., 1992a, Axial imaging through an aberrating layer of water in confocal microscopy, *Opt. Commun*. 88:180–190.

Sheppard, C.J.R., and Gu, M., 1992b, Image formation in two-photon fluorescence microscopy, *Optik* 86:104–106.

Stelzer, E.H.K., Hell, S., Lindek, S., Pick, R., Storz, C., Stricker, R., Ritter, G., and Salmon, N., 1994, Nonlinear absorption extends confocal fluorescence microscopy into the ultra-violet regime and confines the illumination volume, *Opt. Commun*. 104:223–228.

Stelzer, E.H.K., Wacker, I., and De Mey, J.R., 1991, Confocal fluorescence microscopy in modern cell biology, *Semin. Cell. Biol*. 2:145–152.

Török, P., Varga, P., Laczik, Z., and Booker, G.R., 1995, Electromagnetic diffraction of light focused through a planar interface between materials of mismatched refraction indices: An integral representation, *J. Opt. Soc. Am. A* 12:325–332.

Wilson, T., and Sheppard, C.J.R., 1984, *Theory and Practice of Scanning Optical Microscopy*, Academic Press, New York.